IEEE Access
Multidisciplinary | Rapid Review | Open Access Journal

Received 25 July 2022, accepted 29 August 2022, date of publication 8 September 2022, date of current version 20 September 2022.

Digital Object Identifier 10.1109/ACCESS.2022.3205405

RESEARCH ARTICLE

Design and Validation of the Physical Layer Functions of FBMC/OQAM Transceiver With Improved Residual Phase Error Correction

KHALED A. ALAGHBARI, HENG-SIONG LIM, (Senior Member, IEEE), NOR HIDAYATI ABDUL AZIZ, T. BHUVANESWARI, (Senior Member, IEEE), AND TICK HUI OH, (Senior Member, IEEE)

Faculty of Engineering and Technology (FET), Multimedia University (MMU), Bukit Beruang, Melaka 75450, Malaysia

Corresponding author: Tick Hui Oh (thoh@mmu.edu.my)

This work was supported in part by Multimedia University (MMU).

ABSTRACT In this paper, we report experimental results on the development and improvement of the physical layer functions of a filter bank multicarrier with off-set quadrature amplitude modulation (FBMC/OQAM) transceiver using a testbed implemented with programmable software-defined radio (SDR). The developed physical layer approach is similar to the IEEE 802.11a standard, and it has been tested for timing synchronization, carrier frequency offset (CFO) correction, channel estimation and equalization. An investigation into the inherent intrinsic imaginary interference in FBMC/OQAM has been carried out, with initial findings indicating the seriousness of the effect of phase noise (PN). The conventional pilot structure used in IEEE 802.11a cannot be directly applied to FBMC/OQAM, thus, a specially designed pilot scheme is proposed to deal with the residual phase error. Three phase noise estimation schemes have been evaluated, namely phase noise compensation (PNC), extended Kalman filter (EKF) and modified blind phase searching (MBPS) methods. To further suppress the residual interference and enhance the phase error correction, an iterative technique is used after the pilot equalization. The performance of the proposed methods has been evaluated experimentally and via simulation for an indoor environment. The results verify the capabilities of the proof-of-concept transceiver and the developed physical layer functions.

INDEX TERMS FBMC/OQAM, physical layer, phase noise, MBPS, Kalman filter, PNC, ISDF, WARP.

I. INTRODUCTION

Filter bank multicarrier with off-set quadrature amplitude modulation (FBMC/OQAM) system is a potential waveform candidate for future mobile communication. FBMC has recently attracted attention due to its advantages of better spectrum efficiency, lower side-lobes and higher robustness to narrow-band interference over the conventional orthogonal frequency division multiplexing (OFDM) [1], [2]. Despite the advantages of FBMC over OFDM, it has many challenges that limit its implementation. For example, complexity in the system design due to the usage of filter banks at transmitter and receiver compared to OFDM, the time-frequency domain channel estimation requires specially designed preamble to eliminate the intrinsic interference, and advanced equalizer such as N-tap frequency sampling equalizer is usually needed to effectively equalize the channel [3], [4], [5]. Moreover, residual phase error due to CFO requires specially designed pilots protected from the intrinsic interference as well [6].

The mismatch between the local oscillators of the transmitter and receiver create a carrier frequency offset (CFO) and phase noise (PN).These effects give rise to inter-carrier interference (ICI) and common phase error (CPE) in any multicarrier system. ICI destroys the orthogonality between the subcarriers and the CPE causes rotation in the entire constellation [7]. CFO is typically estimated and corrected in the time domain through multiplication with a digital carrier whose frequency negates the CFO estimate. The IEEE

The associate editor coordinating the review of this manuscript and approving it for publication was Luca Barletta.

802.11a standard [8] uses a technique that compares two long training sequential (LTS) preamble symbols to estimate the CFO in a process called coarse CFO estimation. This is followed by channel impulse response (CIR) estimation using LTS preamble and then channel equalization. However, even after CFO correction is done in the time domain, there is typically a residual time-varying phase error (PE) that must be estimated in the frequency domain and tracked over time. Thus, OFDM systems employ multiple pilot subcarriers to estimate and correct the residual PE in the system. It is important to highlight that, pilots are used to estimate the PE after CIR estimation and equalization, therefore accurate channel estimation and equalization are needed. Unfortunately, FBMC/OQAM suffers from intrinsic imaginary interference (IMI) caused by the adjacent subcarriers and symbols [5]. The effect of IMI can be exacerbated by the presence of any complex distortion such as selective fading channel, CFO, PN, etc. [6]. These effects result in additional crosstalk for OQAM, leads to bit-error-rate (BER) floor and degrade the performance of a FBMC/OQAM system [9]. There are many works on CFO and PE estimation and correction for OFDM systems. However, works that are focused on overcoming the impact of selective fading channel, CFO and PE for FMBC are very limited. For instance, [4], [9], [10], [11], [12] discussed PN problem only, [13], [14], [15] discussed CFO and channel estimation, while [16] considered only channel equalization. In this paper, we investigate jointly the impact of several channel impairments and DSP-based compensation techniques mainly CFO, PN, channel estimation and equalization which become more challenging in the real-time demodulation of FBMC/OQAM. This problem, which has not yet been adequately investigated in the literature, needs to be addressed for realizing the full potential of the FBMC/OQAM system.

In [6], a pseudo-pilot was designed to avoid IMI for joint estimation of CFO and PE. In [10], coding and decoding matrices at the transmitter and receiver were utilized to suppress IMI and compensate for PN. In [4], an adaptive maximum likelihood estimator was used for PN compensation. In [11], a pilot-based extended Kalman filter was proposed for PN estimation. In [12], analytical expressions for the interference power under perfect CPE correction of the OQAM symbols were derived. Numerical evaluation showed that FBMC-OQAM is more robust against phase error than OFDM. The authors in [9] proposed a modified blind phase searching (MBPS) method to adapt classical BPS to the OQAM modulation. The modified BPS method makes the classical BPS applicable to OQAM symbols, but BPS-based methods generally have high complexity [6]. The MBPS method is usually used to increase system spectral efficiency since no pilot is needed. The MBPS has been used in many FBMC/OQAM systems to compensate for PN [4], [10], [11].

Estimation of channel CIR and CFO is also a common approach used in previous studies. In [13] and [14], a two-step preamble-based approach was proposed to estimate CFO and CIR in multiple-input-multiple-output (MIMO) FBMC/OQAM system [13] and in single-input-multiple-output (SIMO) FBMC/OQAM system [14]. A coarse CFO estimator which does not require the channel knowledge was used in the first step. Channel estimation based on least squares (LS) estimator and conventional interference approximation method (IAM) was considered in [2], [3], and [14], and a minimum mean square error (MMSE) estimator in time domain was used in [13]. In [15], an improved joint maximum-likelihood (ML) estimation method for CFO, sampling time offset, and CIR was proposed for OFDM/OQAM based on pilots. In [16], an iterative soft decision feedback (ISDF) technique to eliminate the residual inter-symbol interference (ISI) and inter-carrier interference (ICI) was proposed to enhance the equalization for FBMC/QOAM system. The accuracy of PE estimation is highly dependent on the capability of estimating and equalizing the wireless channel distortion.

Despite the promising results of FBMC/QOAM as a candidate waveform for next generation wireless systems, experimental investigation for the physical layer processing of the FBMC/OQAM systems with genuine RF signals generated in real-time while taking into account the three important error sources, namely CFO, PE, and CIR, is still lacking on real-life hardware system. Prior works on SDR-based implementation for FBMC/OQAM are limited. In [17], the authors implemented FBMC transmitter and receiver on two universal software radio peripheral (USRP) N210 boards and MATLAB software. They focus on the practical aspects of time and frequency synchronization of the frames and channel estimation. In [18], a universal physical layer called uPHYLA for uplink FBMC receiver, for single-input single-output (SISO) and multiple-Input multiple-output (MIMO) scenarios, was developed based on USRP2 and GNU Radio. A WiMAX based simulator programmed in MATLAB was developed within the project. The authors in [19] implemented FBMC/OQAM on USRP N310 with GNU Radio, where they concentrated on frequency-domain synchronization issue only. However, in the above works [17], [18], [19], there is no detail analysis of the joint impact of CFO, residual CFO, channel estimation and equalization on the FBCM/OQAM transceiver.

In this paper, the physical layer function of the FBMC/OQAM system is implemented on WARP (wireless open-access research platform) hardware. WARP is a software-defined radio (SDR) platform developed by Rice University and Mango Communications [20], [21]. Version 3 of the WARP kit is built on a Xilinx Virtex-6 LX240T FPGA with two programmable radio frequency (RF) interfaces operating at 2.4 or 5 GHz with a 40 MHz bandwidth [21]. The reference design of the WARP kit implements the MAC and PHY from the 802.11a/g standard. It combines MATLAB and FPGA implementations of the WARP framework modules to allow different physical layer designs to be constructed and tested. The reference design uses MATLAB to control nodes and perform signal processing. So far, there is no other work on the implementation of FBMC/OQAM on the WARP kit.

In this work, the FBMC/OQAM physical layer functions including symbol timing acquisition, carrier frequency offset (CFO) correction, channel estimation, equalization, and residual phase error compensation are experimentally evaluated. The proposed physical layer structure is similar to the IEEE 802.11a standard; moreover, to combat the IMI inherent in FBMC/OQAM, two pilots protected with zeros are designed for phase error estimation. An iterative technique is proposed to eliminate the residual interference and enhance the phase error compensation. The core contribution of this paper is the SDR-based hardware-in-the-loop over-the-air evaluation and optimization of timing and frequency synchronization as well as channel estimation procedures of a FBMC/OQAM waveform with specially designed preamble and pilot symbols. This paper is organized as follows: the FBMC/OQAM system modeling and its implementation on WARP are introduced in Section 2; the phase error estimation and compensation methods are described in Section 3; discussion of experiment and simulation results is presented in Section 4; finally, the conclusion is drawn in Section 5.

II. SYSTEM MODEL

A. FBMC/OQAM SYSTEM MODEL

Fig. 1 illustrates the FBMC/OQAM system model. At the transmitter, QAM symbols $c_m(p)$ are generated and converted into offset QAM (OQAM) symbols, where the real and imaginary values of the QAM symbols are staggered to form real-valued symbols $d_{m,n}$. The symbols are then multiplied by a phase factor $e^{j\varphi_{m,n}} = e^{j(m+n-2mn)\pi/2}$ to obtain orthogonal OQAM symbols, upsampled by factor of $M/2$ and filtered by using synthesis filter banks (SFB), where M is the number of subcarriers. In this work, the PHYDYAS prototype filter $g(l)$ [22], [23] is applied with overlapping factor $K = 4$ and length $L_g = KM$. The synthesis filter banks (SFB) and analysis filter banks (AFB) can be efficiently implemented by the combination of polyphase network (PPN) and fast Fourier transform (FFT). The resulting FBMC signal is given by [6], [11]:

$$s(l) = \sum_{m=0}^{M-1} \sum_{n=0}^{N-1} d_{m,n} g_{m,n}(l) e^{j\varphi_{m,n}} \tag{1}$$

where $g_{m,n}(l) = g\left(l - n\frac{M}{2} - \frac{L_g-1}{2}\right) e^{j\frac{2\pi}{M}m\left(l-\frac{L_g-1}{2}\right)}$, while the parameters M, m, and n represent the number of subcarriers, subcarrier index, and time index respectively. The received signal is then filtered by the analysis filter bank (AFB). Denoting $h(l)$ as the channel impulse response and $w(l)$ as the additive white Gaussian noise (AWGN) samples, the input signal to AFB can be written as [6], [24]:

$$y(l) = (h(l) * s(l)) e^{j(2\pi \Delta f l + \varphi(l))} + w(l) \tag{2}$$

$$\varphi(l) = \varphi(l-1) + \varepsilon(l) \tag{3}$$

where $*$ is the convolution operator defined as $h(l) * s(l) = \sum_{k=-\infty}^{\infty} h[k]\, s[l-k]$, Δf is the normalized CFO, $\varphi(l)$ is the phase noise (PN) which can be modelled as a Wiener process [25], [26], and $\varepsilon(l)$ is a sequence of independent and identically distributed (i.i.d) Gaussian random variables with zero mean and variance of σ^2. The demodulated signal on the m_0-th subcarrier at the n_0-th time instant, assuming the channel frequency response (CFR) is almost flat over the neighborhood of subcarrier m_0, is expressed as in (4), shown at the bottom of the page, [6], where $ju_{m_0,n_0} = \sum_{(m,n)\neq(m_0,n_0)} d_{m,n} \sum_{l=0}^{L_g-1} g_{m,n}(l)\, g^*_{m_0,n_0}(l)$ is the additional crosstalk caused by intrinsic imaginary interference (IMI), and the prototype filter used in (4) is assumed to exhibit good spectral containment so the crosstalk is mainly caused by the

$$\begin{aligned}
y_{m_0,n_0} &= \sum_{l=0}^{L_g-1} y(l)\, g^*_{m_0,n_0}(l) e^{-j(m+n-2mn)\frac{\pi}{2}} \\
&= \sum_{l=0}^{L_g-1} \Big[H_{m_0} e^{j(2\pi \Delta f l} \\
&\quad + \varphi(l)) s(l) + w(l) \Big] g^*_{m_0,n_0}(l)\, e^{-j(m+n-2mn)\frac{\pi}{2}} \\
&= \sum_{l=0}^{L_g-1} \left[H_{m_0} e^{j(2\pi \Delta f l + \varphi(l))} \sum_{m=0}^{M-1} \sum_{n=0}^{N-1} d_{m,n} g_{m,n}(l) e^{j(m+n-2mn)\frac{\pi}{2}} + w(l) \right] g^*_{m_0,n_0}(l) e^{-j(m+n-2mn)\frac{\pi}{2}} \\
&= \sum_{l=0}^{L_g-1} \left[H_{m_0} e^{j(2\pi \Delta f l + \varphi(l))} \sum_{m=0}^{M-1} \sum_{n=0}^{N-1} d_{m,n} g_{m,n}(l)\, g^*_{m_0,n_0}(l) + w'(l) \right] \\
&\cong H_{m_0} d_{m_0,n_0} e^{j(2\pi \Delta f n_0 + \varphi(n_0))} \\
&\quad + H_{m_0} \sum_{(m,n)\neq(m_0,n_0)} d_{m,n} \sum_{l=0}^{L_g-1} g_{m,n}(l)\, g^*_{m_0,n_0}(l)\, e^{j(2\pi \Delta f n_0 + \varphi(n_0))} + w'_{m_0,n_0} \\
&\cong H_{m_0} e^{j(2\pi \Delta f n_0 + \varphi(n_0))} \left(d_{m_0,n_0} + j u_{m_0,n_0} \right) + w'_{m_0,n_0}
\end{aligned} \tag{4}$$

adjacent subcarriers $m \pm 1$ [2], [5]. Based on (4) it is clear that the data symbol d_{m_0,n_0} is affected by channel, CFO and PN in addition to the IMI. If the system is ideal and there are no channel, CFO and PN distortions, the real-valued symbol d_{m_0,n_0} can be recovered by simply taking the real component of (4). However, this is not true in the presence of channel distortion, CFO and PN. Hence, estimation and compensation of these effects before the demodulation in the FBMC is necessary.

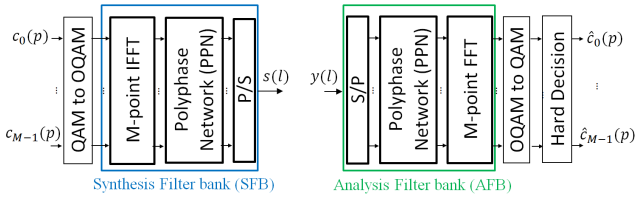

FIGURE 1. Structure of the FBMC/OQAM system.

B. IMPLEMENTATION OF THE PROPOSED FBMC/OQAM SYSTEM ON WARP

The structure of the FBMC/OQAM frame is designed to be similar to the IEEE 802.11a standard that is used in the WARP kit for 64-subcarrier OFDM system, where only the pilot and data subcarrier locations are changed.

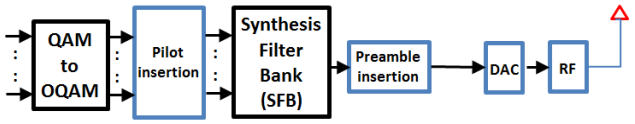

FIGURE 2. FBMC/OQAM transmitter implemented on WARP kit.

The block diagram of the FBMC/OQAM transmitter is depicted in Fig. 2. After obtaining OQAM symbols from QAM symbols, two pilots at subcarrier locations {27, 39} are inserted as shown in Fig. 3b. These subcarriers are protected by zero padded subcarriers at location {25, 26, 40, 41} to avoid IMI in the FBMC/OQAM system. The pilot tone values are defined as BPSK symbols $\{+1, -1\}$ that are repeated across all FBCM/OQAM symbols. These pilots are needed to estimate the residual CFO which causes a time varying phase offset that increases linearly with each FBMC symbol. The OQAM data are mapped to subcarriers located at {2:24, 42:64}, with a total of 46 subcarriers for the useful data. The remaining subcarriers are set to null. Then the SFB is applied to each subcarrier and the outputs are combined to form the time-domain FBMC/OQAM signal. The preamble is then appended to this signal as shown in Fig.3a. Each FBMC/OQAM frame contains preamble for detection, synchronization, coarse CFO estimation and channel estimation purposes. This preamble (640 samples) consists of two parts known as short training symbols (STS) and long training symbols (LTS), which are known at both sides of the communication link. The STS is intended for signal detection, automatic gain control (AGC) stabilization and diversity (if several antennas are used).The STS of length 480 samples, as shown in Fig. 3c, is formed by repeating 30 times a 16-digit pattern of BPSK symbols and zeros. The LTS with 160 samples is formed through repeating 2.5 times the time-domain sequence of the 64-sample sequence in Fig. 3d. The LTS is used for timing synchronization, coarse CFO estimation and channel estimation. The source code for implementing FBMC/OQAM on WARP kit can be found in [27].

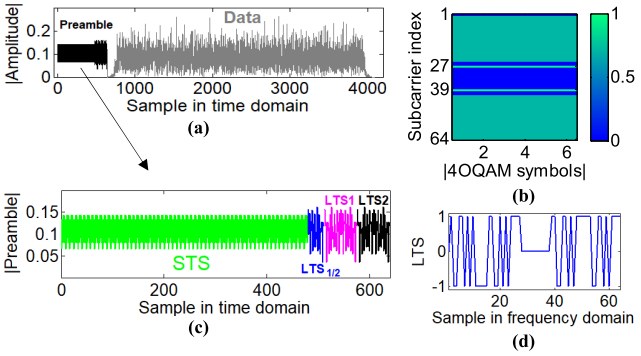

FIGURE 3. Structure of the FBMC/OQAM frame in (a) time domain (b) frequency-time domain, (c) preamble signal, (d) LTS pattern before IFFT.

The FBMC/OQAM data to be transmitted have to be interpolated by rate of 2 and padded with zeros in order to match the buffer size of the WARP kit, as the buffer size of each radio board is about 2^{14}. The signal is then scaled between -1 and +1. The FBMC/OQAM signal, which consists of time domain samples with real (I) and imaginary (Q) components, is given as an input to the WARP kit. They are stored separately in I and Q buffer. The stored signal is converted into analog waveforms using a digital-to-analog converter (DAC). The baseband signal is up-converted to an RF carrier frequency of 2.4GHz with 40MHz bandwidth; then, the modulated signal is amplified using RF amplifier and transmitted via the selected antenna.

Fig. 4 shows the FBMC/OQAM receiver. The received signal is down-converted from RF band to baseband and down-sampled by two to match the hardware bandwidth. The LTS preamble is extracted from the received signal for timing synchronization via a cross-correlator. The resulting two LTS correlation peaks establish the timing for the rest of the reception. Since the LTS preamble consists of 2.5 repetition of a 64-sample sequence, two LTSs (LTS1 and LTS2) are used to estimate the CFO by comparing their phases. The CFO ($\Delta\hat{f}$) is estimated by averaging the 64 phase comparisons, then it is removed by multiplying the whole received signal with $exp(-j2\pi\,\Delta\hat{f}\,n)$. The LTS1 and LTS2 preambles are re-extracted again for channel estimation, and then a 64-point FFT is applied to each preamble to obtain two training symbols. The complex channel coefficient is estimated for each non-zero subcarrier by averaging the least squares estimates from the two training symbols. The estimated channel is then fed into a zero-forcing equalizer to

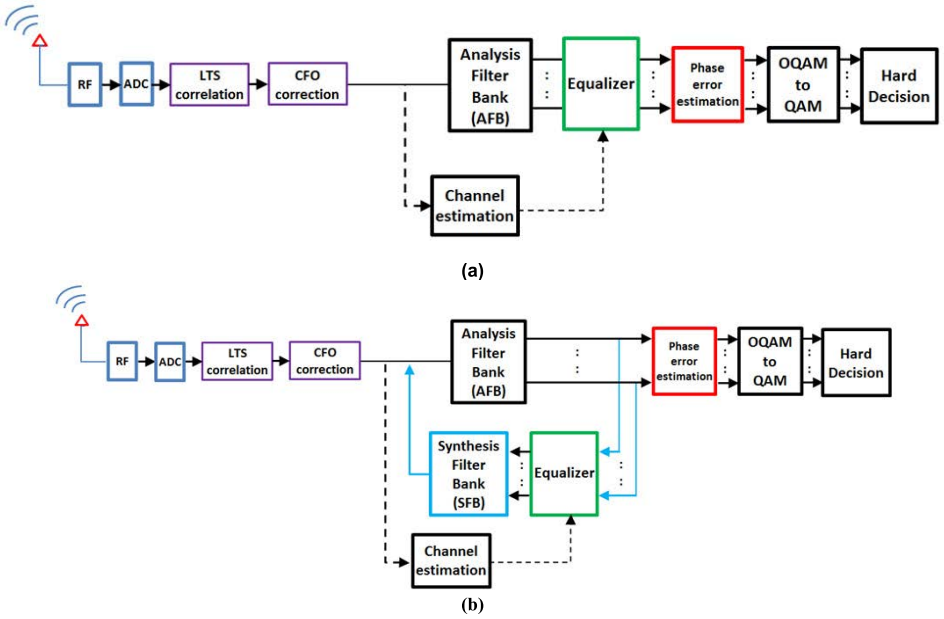

FIGURE 4. (a) FBMC/OQAM receiver implemented on WARP kit (b) Proposed enhanced FBMC/OQAM receiver implemented on the WARP kit.

remove distortion incurred by propagation through the wireless channel as illustrated in Fig. 4a. Before that, the received FBMC/OQAM signal is sent to AFB for match filtering and reshaping into parallel subcarriers. An equalizer is applied to the AFB output that contains the data subcarriers and pilot subcarriers. At this stage the FBMC/OQAM signal still suffer from residual ICI and ISI interference and phase error. The pilot tones embedded in each FBMC/OQAM symbol are extracted to estimate the phase error. Every subcarrier in the FBMC/OQAM symbol is then de-rotated by using the estimated phase error. Unfortunately, the pilots are affected by residual ISI, ICI and noise, thus the phase error estimation accuracy degrades. The zero-forcing equalizer is incapable of restoring the orthogonally of the pulse on the real field and to make things worse, it may enhance the residual interference and noise due to the zero-forcing nature of the simple equalizer. To enhance the phase error estimation and data equalization, the ISDF technique [16] is proposed to be implemented after the equalizer to remove the residual interference from the FBMC/OQAM symbol as illustrated in Fig. 4b. In the proposed FBMC/OQAM system, synthesis-analysis filter banks are used to combat the residual interference and noise. The equalized signal, which is a complex-valued signal that includes the signal and ISI/ICI, is first sent to SFB to re-synthesize the time-domain FBMC/OQAM signal. Through SFB, the interference and noise are spread out and averaged over the entire bandwidth. The output is then passed to AFB to filter out the residual interference and noise for each subband and produce a clean signal. The pilots are then extracted to estimate the phase error more effectively.

C. RESIDUAL PHASE ERROR COMPENSATION TECHNIQUES

Following the approximation model given in (4), the received pilot after AFB is given by:

$$\hat{P}_{m_p,n_p} \cong H_{m_p} e^{j\varphi(n_p)} \left(P_{m_p,n_p} + ju_{m_p,n_p}\right) + w'_{m_p,n_p} \tag{5}$$

where $ju_{m_p,n_p} = \sum_{(m,n)\neq(m_p,n_p)} P_{m,n} \sum_{l=0}^{L_g-1} g_{m,n}(l)\, g^*_{m_0,n_0}(l)$. Similar to the received data symbols the above model shows that the received pilots are also affected by residual phase error and additional crosstalk. In the following section, three important phase error estimation or correction schemes that can be applied to the proposed FBMC/OQAM system are discussed.

1) PHASE NOISE COMPENSATION (PNC) TECHNIQUE

In OFDM [28], [29], [30], assuming the flat and time-invariant channel response on each subcarrier is estimated and corrected perfectly, the phase error can be estimated from known pilots P_{m_p,n_p} by taking the phase of the averaged results of the multiplication of the known pilots with the received pilots $\hat{P}_{m_p,n_p}$ as follows [28]:

$$\hat{\varphi}(n) = arg\left(\frac{1}{M_p}\sum_{m_p=1}^{M_p} \frac{\hat{P}_{m_p,n_p} P^*_{m_p,n_p}}{\left|\hat{P}_{m_p,n_p} P_{m_p,n_p}\right|}\right) \tag{6}$$

where $(\cdot)^*$ is the complex conjugate operator and M_p is the number of pilots. The accuracy of the above model depends on the number of pilots used in the estimation; therefore, there exists a trade-off between the spectral efficiency (SE) and accuracy. In FBMC/OQAM, if the noise term is ignored and

the CFO and wireless channel are assumed to have been efficiently estimated and corrected for all symbols, the received pilot is simplified as [10]:

$$\hat{P}_{m_p,n_p} \cong e^{j\varphi(n_p)} \left(P_{m_p,n_p} + ju_{m_p,n_p}\right) \tag{7}$$

and the phase error estimation becomes [10]:

$$\hat{\varphi}(n) = arg\left(\frac{1}{M_p}\sum\nolimits_{m_p=1}^{M_p} \frac{\hat{P}_{m_p,n_p}\left(P_{m_p,n_p} + ju_{m_p,n_p}\right)^*}{\left|\hat{P}_{m_p,n_p}\left(P_{m_p,n_p} + ju_{m_p,n_p}\right)\right|}\right) \tag{8}$$

Eq. (8) shows the pilots are still affected by IMI. Unfortunately, in practice there is no way to know the associated interference term as they are data-dependent [10]. Hence, in order to employ this simple technique, the interference terms need to be suppressed first. The ISDF technique can be employed to remove the interference term and enhance phase error estimation. The effect of phase error can then be cancelled by multiplying the equalized samples with $exp(-j\hat{\varphi}(n))$.

2) EXTENDED KALMAN FILTER (EKF)

Due to the nonlinear (exponential) component presented in (7), a linear Kalman filter cannot be used directly to estimate the phase error; therefore, an extended Kalman filter (EKF) is normally adopted in this case [11], [31]. At first, the EKF linearizes the measuring equation by taking the first derivative with respect to the phase variable. Eq. (7) and Eq. (3) can be seen as a set of measuring and process equations for the Kalman state-space model. The phase variation $\varphi\left(n_p\right)$ is the state that we want to estimate, while $\hat{P}_{m_p,n_p}$ represents the observable variable which is a complex signal after channel equalization. The procedures for implementing EKF are presented in Fig. 5. The Q and R are the covariance of the processing noise and measuring noise respectively. Kalman gain K_n is updated every iteration from the measurement rather than the noise parameters; therefore the performance of the EKF is not very sensitive to the accuracy of Q. The phase error can be estimated using the known pilot P_{m_p,n_p}. Variables with notation $(n|n)$ denote the posteriori estimation of the current state when the current observation n is available, and variables with notation $(n|n\text{-}1)$ denote the priori estimation of the current state while only having measurements from one past state n-1 available [11].

3) MODIFIED BLIND PHASE SEARCHING (MBPS)

The modified blind phase searching (MBPS) method is a blind method that does not need pilots to correct the phase error. The MBPS method increases the system spectral efficiency (SE), but requires high computational complexity.

The basic idea behind the MBPS method for FBMC/OQAM signal is to pre-rotate the channel equalized signal $z_{m,n}$ with a number of phase tests $\varphi_b = (b/B)\cdot\pi - \pi/2$ before applying the standard OQAM conversion, where $b = 1, 2, \ldots, B$ and B is the total number of phase tests [9]. The rotated nth sample of the kth subcarrier is given by

1) **Input variables:**
   - Received/equalized pilot signal $\hat{P}_{m_p,n_p}$
   - Corresponding transmitted pilot P_{m_p,n_p}
   - Predication noise matrix Q
   - Measurements noise matrix R
2) **Initialization:**
   - Initial phase noise $\varphi(0) = 0$
   - Initial predication error covariance $P(0)$
3) **for n = 1, 2, ...**
   - Predication process:
     - $\hat{\varphi}_{n|n-1} = \hat{\varphi}_{n-1|n-1}$ (Priori state predication)
     - $\hat{P}_{n|n-1} = \hat{P}_{n-1|n-1} + Q$ (Predication error covariance)
   - Measurement process:
     - $\hat{z}_{n|n-1} = P_{m_p,n_p} e^{-j\hat{\varphi}_{n|n-1}}$ (Measurement expectation)
     - $e_n = \hat{P}_{m_p,n_p} - \hat{z}_{n|n-1}$ (Error from the real measurement)
     - $K_n = \left(\hat{P}_{n|n-1} c_n^H\right)/\left(c_n \hat{P}_{n|n} c_n^H + R\right)$ (Kalman gain)
       where $= -j\hat{z}_{n|n-1}$
     - $\hat{\varphi}_{n|n} = \hat{\varphi}_{n|n-1} + K_n e_n$ (Update the predication by Kalman gain)
     - $\hat{P}_{n|n} = \hat{P}_{n|n-1}(1 - K_n c_n)$ (Update the error covariance)

FIGURE 5. Procedure of EKF for estimating the phase error using pilots.

$z_{m,n,b} = z_{m,n} \cdot exp\left(j\varphi_b\right)$. The subcarrier index m in $z_{m,n,b}$ can be omitted to simplify the notation to $z_{n,b}$. The rotated phase is selected such that the given cost function is minimized. The effect of the additive noise can be reduced by averaging the cost function over $2N$ consecutive samples with the same phase test φ_b. The estimated phase rotation with respect to the PN suppression can be written as [31]:

$$\hat{\varphi}_{b,MBPS} = \arg\sum\nolimits_{i=-N}^{N-1}\left(\left|z_{n+i,b} - DD\left(z_{n+i,b}\right)\right|^2\right) \tag{9}$$

where DD is a direct decision operator.

III. RESULTS AND DISCUSSION

A. EXPERIMENT SETUP AND RESULTS

The evaluation of the proposed FBMC/OQAM system is performed using two WARP v3 kits operating at 2.412 GHz, which are connected through a gigabit Ethernet switch to a personal computer (PC). MATLAB is used for constructing the transmitted FBMC/OQAM signal and performing the signal processing techniques for the received signal. Fig. 6 shows the layout of the experimental setup. The field measurements have been carried out along the corridor on the 2nd floor of Faculty of Engineering and Technology (FET), Multimedia University (MMU). The corridor is 50m in length, 4.5m in width and 4m in height on one side and 18m in height on other side as shown in Fig. 6. The side walls, floor and ceiling of the corridor are constructed of concrete/bricks with cement plaster on the surface; the floor is covered with polished concrete. There are some plastic chairs, tables, wooden doors and some windows in the corridor. There are two semi-open space with 2m in width on both sides of the corridor. In the measurements, the windows were closed; only one lab door was open. The transmitter (TX) board is placed at the height of 1.6m, at the location denoted by the solid square in Fig. 6. The receiver (RX) board is placed at the height of 0.75m, and moved along the straight dashed line.

To investigate the importance of the residual phase error correction process, the constellation of the received FBMC/OQAM symbols with channel equalization only is shown in Fig. 7a, where the Tx-Rx separation is less

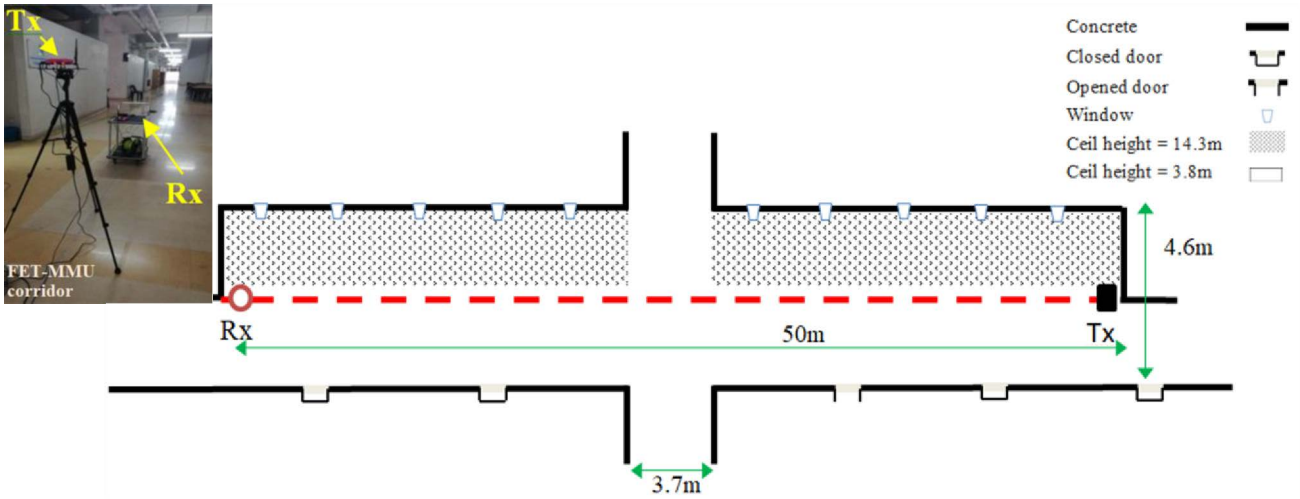

FIGURE 6. FET-MMU Corridor layout of the experimental setup.

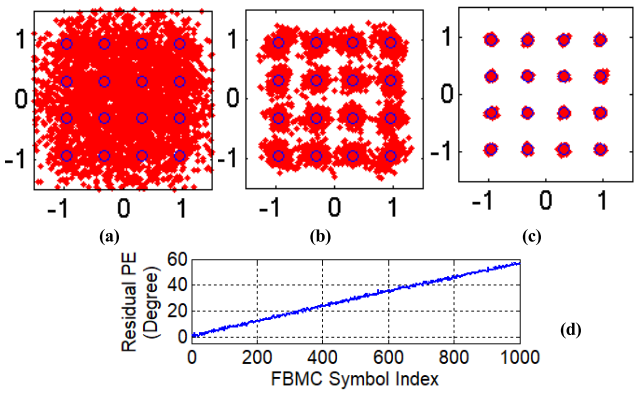

FIGURE 7. Constellation diagram of the received FBMC with 16OQAM symbols with (a) channel equalization only (b) CFO and channel equalization (c) CFO, channel equalization and residual phase error correction, (d) Phase error estimation over FBMC symbol in degree.

than 0.5m. It can be observed that the symbols are scattered all over the constellation plot because they are severely contaminated by other distortions such as CFO and residual phase error. Fig. 7b illustrates the constellation diagram after performing CFO correction and channel equalization where the constellation points are less contaminated; however, the error rate of the FBMC/OQAM system is still high. Next, with additional phase error correction, the constellation points become clearer and the FBMC/OQAM system is almost error-free as shown in Fig. 7c. It is important to stress that channel estimation and equalization are not enough to recover the FBMC symbols, there are still CFO and residual CFO that need to be estimated and corrected. The time domain CFO estimator seeks to minimize the impact of ICI by reducing the CFO before samples are fed into the receiver's AFB. However, this estimator will rarely remove all CFO, leaving a residual CFO which causes a time varying phase offset. The pilots are used to estimate and correct this residual phase error. The channel estimation can be done efficiently, since the 16QAM symbols are correctly recovered after phase error correction. The estimated coarse CFO is 447.7Hz and estimated phase error (residual CFO) is 38.4Hz, which lead to an overall CFO of 486.1Hz corresponding to 0.20 ppm (parts per million). Even though the residual CFO is small, it has significant impact because it causes phase offsets which increase from zero (at the start of the packet) to 57.2° (at the end of the packet) as shown in Fig. 7d. For 16QAM, the inner symbols can tolerate 45° phase shift, however, the outer symbols can tolerate only 16.8°. The WARP v3 transceiver is designed based on TCXO oscillator, which has frequency accuracy of ±2.5 ppm (i.e., maximum CFO is ±12kHz at carrier frequency of 2.4GHz). In comparison with other USRPs such as NI-USRP- 2920, 2921, 2922 and USRP N210 a frequency accuracy of ±2.5 ppm is also being specified, however, USRP N310 provides better frequency accuracy of ±0.1 ppm (corresponding to maximum CFO of ±480Hz at carrier frequency of 2.4GHz). It is important to mention that the IEEE 802.11a specification has suggested oscillator precision tolerance up to ± 20 ppm, which allows for much higher clock deviation of the oscillators.

We examined the distortion accumulated on the protection pilot located at subcarrier 26 and the results are depicted in Fig. 8. The received signal "Rx" (green) contains the distortion of the channel, CFO and additive noise. By applying CFO correction and channel equalization we get the signal "Rx after equalizer" (red), where it can be observed that the magnitude of distortion has been reduced. This signal represents the approximate sum of residual phase error and residual interference, provided the additive noise is small and the channel impulse response is correctly estimated (this assumption is valid for the near error-free scenario described in Fig. 7). The residual distortion can be reduced further by employing ISDF technique as presented in Fig. 8.

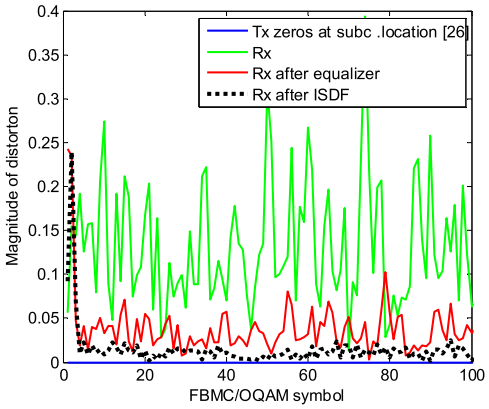

FIGURE 8. The accumulated distortion on the protection pilot.

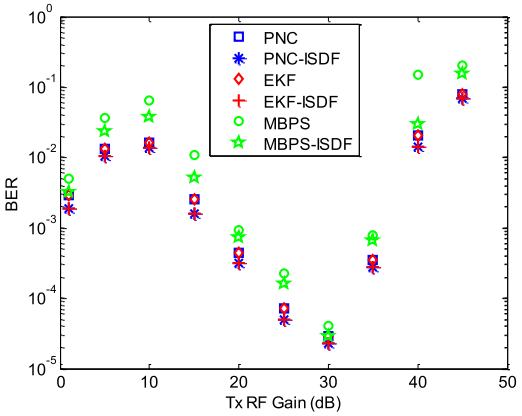

FIGURE 9. BER versus the RF gain of the FPGA board used as transmitter.

For the WARP kit, the power of the transmitted signal can be adjusted through the baseband (BB) gain and RF gain with gain range of 0-3dB and 0-63dB respectively. Using MATLAB, the values of these parameters can be adjusted to get a particular gain. The power of the received signal can be set to automatic or manual. The automatic setting turns the AGC on, where the AGC is designed to optimize the Rx BB and RF gains so that the analog signal presented to the ADC is within the dynamic range of the ADC. If AGC is disabled, then the user must select the Rx gains that result in a good signal level at the ADC input. Fig. 9 shows the Tx RF gain versus BER performance that is evaluated in the experiment with the Tx BB, Rx BB and Rx RF gains fixed to 3dB, 12dB and 2dB respectively. Based on the average of 30 data measurements, all algorithms achieve their best BER performance with Tx RF gain at about 30dB. The transmitted power from the RF antenna of the WARP kit is calibrated by connecting the RF interface to a spectrum analyzer using a coaxial cable with 5 dB loss and transmitting the FBMC/OQAM signal at Tx RF gain of 30dB. The measured transmitted power is 6dBm, corresponding to 30dB gain. The performance of different techniques to eliminate the phase error have also been tested and shown in Fig. 9. The phase error estimation and correction based on PNC shows similar performance with the EKF-based method. The two methods outperform the MBPS-based method. The ISDF technique further improves the performance of the three algorithms.

In order to characterize the propagation environment in the FET-MMU corridor, a measurement experiment has been conducted where a continuous signal power of 6dBm at 2.412GHz generated by a function generator is measured by a spectrum analyzer for different Tx-Rx separation distances as shown in Fig. 10a, the measurement data can be found in [32]. The received power for four measurements versus the distance between the transmitter and receiver are plotted in Fig. 10b. To obtain more insight about the propagation of wireless channel in the corridor, the ray-tracing technique [33], [34], [35] is used. The technique computes the power and delay of the line-of-sight (LoS) ray and reflected rays caused by external objects such as walls and floor, considering the dimensions of the corridor and the position of Tx and Rx. The received power based on the theoretical free-space path loss (FSPL) and ray tracing with four paths are plotted for comparison. It can be observed that the received signal power is similar to the simple line-of-sight condition for distance up to about 10 m. At certain locations between the Tx and Rx, the signal experience deep fade due to multipath effects, where this phenomenon is very well represented with ray tracing of four paths compared with FSPL. Therefore, the FBMC/OQAM received signal is expected to have power drops in some locations.

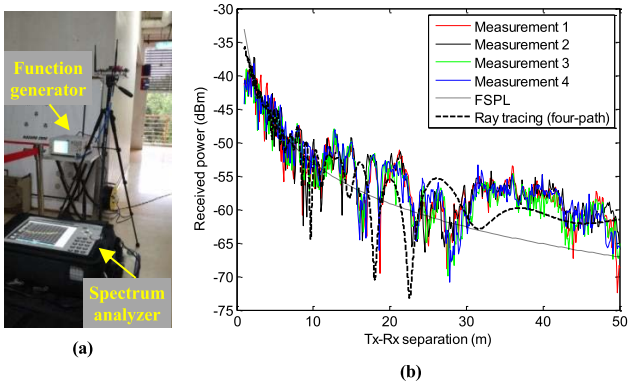

FIGURE 10. (a) Instruments (function generator and spectrum analyzer) used to measure the path loss, (b) Received signal power (dBm) versus the distance (meter) between Tx and Rx.

In this experiment the wireless channel between the transmitter and receiver exhibits Rician fading. Fig. 11 shows an example of the power delay profile (PDP) for a separation distance of 10m. The first peak is due to the LoS path from Tx to Rx. The RMS delay spread of the example shown in Fig. 11 is 1ns.

The performance of the three phase error compensation techniques is evaluated for different distances between the Tx and Rx and the results are depicted in Fig. 12. The transmitter is fixed at one location and the receiver station is moved

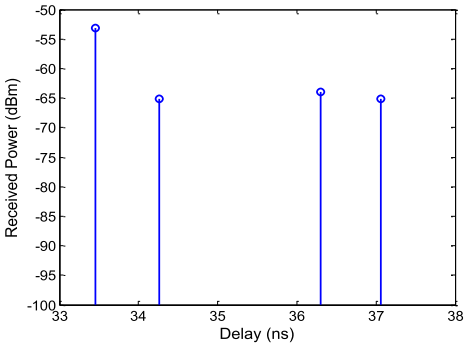

FIGURE 11. Power delay profile (PDP) for Tx-Rx separation of 10 meter.

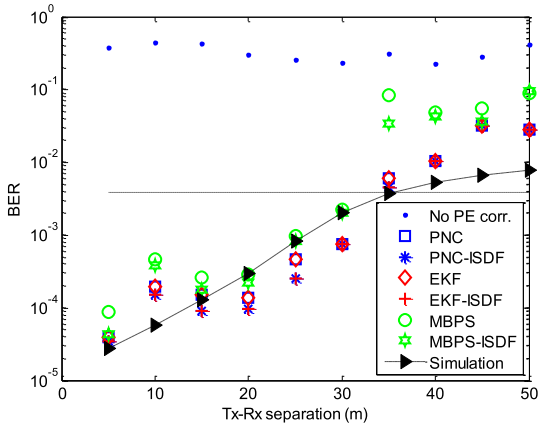

FIGURE 12. BER versus different distance between transmitter and receiver FPGA boards.

to different distances along the dashed line as illustrated in Fig. 6. The channel estimation method used in this system works well so channel distortion is not a big problem. However, Fig. 12 shows that without the PE correction method, the BER performance is degraded very much; this is because of the existence of the phase noise that causes the received symbols to be rotated, and also the existence of the crosstalk introduced by the IMI. Implementing PE compensation techniques can significantly improve the BER performance as shown in Fig. 12. The fluctuation of the BER curve is due to multipath fading effects caused by the wireless channel, as shown earlier in Fig. 10b. Fig. 12 demonstrates that the algorithms work well up to 30 meters, then their performances start to degrade beyond the FEC limit of 3.8×10^{-3} [36]. The PNC and EKF-based methods provide better performance than MBPS. The performance of PNC and EKF are almost the same because the EKF is independent of the noise covariance. The ISDF technique enhances the PE correction in the three methods because it has the capability to combat the residual IMI caused by the channel distortion. Further investigation will be carried out to gain further insight and the results are presented in the simulation section. The simulation of the FBMC/4OQAM system is carried out based on four-path ray-tracing model derived earlier, where different K-factors are used at each distance. The experimental BER results agree well with that of the simulation.

B. SIMULATION RESULTS

To explore the advantages of the proposed system the following simulations have been conducted. The indoor channel model is simulated based on specifications given in [37]. Two channel models are used in this part, namely model B with 15 ns rms delay spread and model C with 30 ns rms delay spread for a typical residential home and small office. Fig. 13 highlights the results of testing the performance of the FBMC/4OQAM (solid lines) and OFDM (dashed lines) systems under different channel models: model B, model C and the corridor PDP as given in Fig. 11 with delay spread of 1.34ns. The results are compared with cases involving AWGN (additive white Gaussian noise) channel and no CIR estimation. The BER performance of the system based on the corridor PDP model is better because it has a relatively smaller delay spread compared to models B and C. Models B and C consider much richer scattering NLoS environment (i.e., more and longer reflected paths), therefore the frequency selectivity of the channels is higher compared with the FET-MMU corridor model. The OFDM outperforms the FBMC/OQAM in AWGN scenario; however, when the channel experiences a multipath effect as in practical scenario, the FBMC/OQAM performs better than OFDM under severe multipath channel models as in model B and C, and slight improvement in FBMC/OQAM can be achieved in moderate multipath model as in MMU-FET corridor.

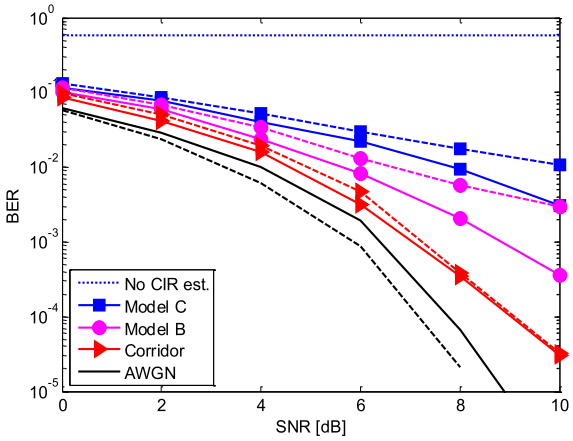

FIGURE 13. BER performance of FBMC/OQAM (solid lines) and OFDM (dashed lines) systems under different channel models.

The performances of BER of the PNC and EKF methods are investigated at SNR of 10 dB, for two phase errors with variances of $\sigma^2 = 0.15\times10^{-3}$ (solid line) and 1.42×10^{-3} (dashed line) using channel model B, the PN values are selected to show the performance difference of the PN correction algorithms under moderate and high phase error, where the obtained results are illustrated in in Fig. 14. The BER under different pilot-to-signal-power-ratios (PSRs) is shown

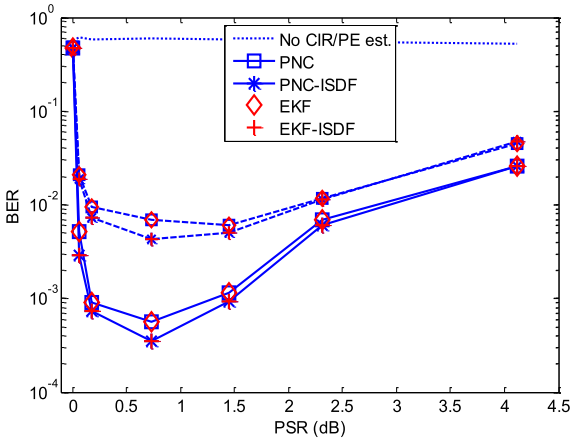

FIGURE 14. BER as function of pilot-to-signal-power-ratio (PSR), at SNR of 10dB, channel model B and phase error variance of $\sigma^2 = 0.15\times10^{-3}$ (solid line) and 1.42×10^{-3} (dashed line).

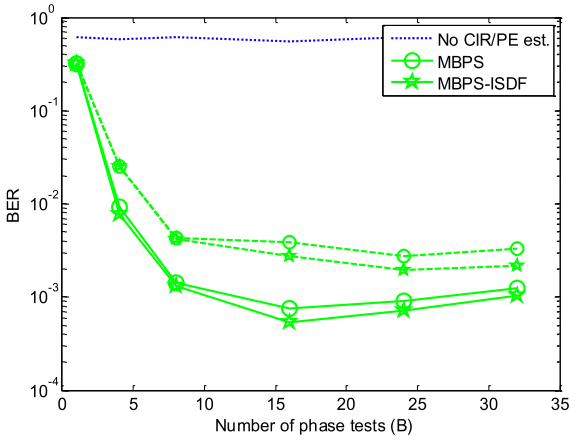

FIGURE 15. BER as function of number of phase tests (PSR) for MBPS-based methods, at SNR of 10dB, channel model B and phase error variance of $\sigma^2 = 0.15\times10^{-3}$ (solid line) and 1.42×10^{-3} (dashed line).

in Fig. 14. The PSR is defined as:

$$PSR = 10\log_{10}(P_p/P_s) \tag{10}$$

where P_p is the FBMC/4OQAM signal power containing the pilot tones, and P_s is the FBMC/4OQAM signal power without pilots. The figure shows that when no CIR or PE estimation is implemented, the system fails. Using the channel and PE estimation techniques that are described earlier in Section 2.B improves the system performance. In the low PSR region, the BER decreases as the PSR increases. This is because the higher power allocated for the pilots makes them easier to be estimated at the receiver. When the pilot power is very small compared to the FBMC/4OQAM signal, the noise distorts the pilots and causes degradation in BER performance. However, we also found that the BER performance degrades when the PSR is higher than 0.75. This is due to the fact that more power is allocated to the pilots and the power allocated to the useful data decreases, hence making the data more vulnerable to noise effects. Fig. 14 also shows that when using ISDF technique on PNC and EKF, the performance of BER decreases. Hereafter, the best PSR found in Fig. 14 is used to evaluate the performance of the proposed system.

Fig. 15 shows the BER performances of MBPS and ISDF-MBPS that are evaluated for different number of phase tests, B. The number of phase tests is important to rotate the equalized signal and minimize the cost function as discussed earlier in Section C.3. Increasing the number of phase tests increases the computational complexity extensively; therefore it is important to optimize this parameter to choose the best number of tests that provides a good performance. The MBPS based methods are tested at SNR of 10 dB, for two phase errors with variances of $\sigma^2 = 0.15\times10^{-3}$ (solid line) and 1.42×10^{-3} (dashed line) using channel model B, as shown in Fig. 15. The MBPS and MBPS-ISDF methods provide good BER performance when the number of phase tests is greater than 8. The MBPS-ISDF method performs better than the MBPS, this is because the IMI coming from neighbouring symbols deteriorates the data symbol

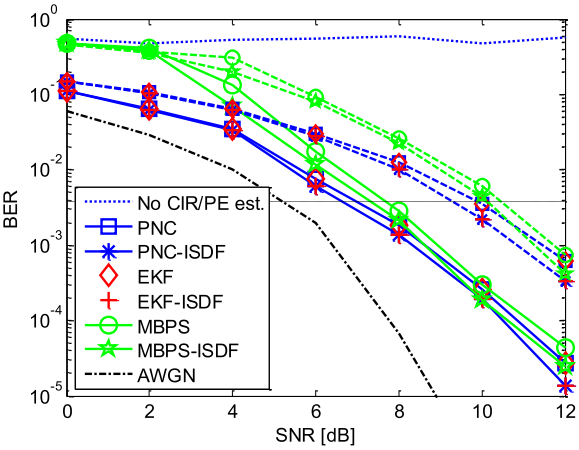

FIGURE 16. BER versus SNR at phase error variance of $\sigma^2 = 0.63\times10^{-3}$ in channel model B (solid line) and channel model C (dashed line).

detection accuracy. Thus, eliminating the residual IMI using ISDF technique enhances the PE correction.

The BER versus SNR plot is given in Fig. 16. Firstly, the simulation result for AWGN (additive white Gaussian noise) with the assumption of no channel and phase error effects is presented. The performances of the methods are tested at phase error variance of $\sigma^2 = 0.63\times10^{-3}$ for two channel models, model B (solid line) and model C (dashed line). At low SNR, the PNC and EKF-based methods perform better than the MBPS-based methods. The ISDF technique enhances the performance further, where the enhancement gets better as the SNR increases, because at low SNR, the noise effect is more dominant than the signal power and the additional IMI cannot be removed. The MBPS method performs better at higher SNR, and its performance is close to the PNC and EKF's performance. This is because the MBPS-based method can average the noise influence when calculating the PE error. When the channel distortion is higher as in model C (dashed line), because of the higher delay spread compared to channel model B, the ISDF-based methods show

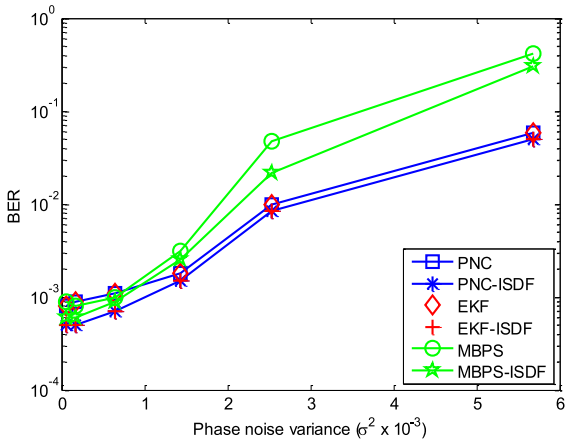

FIGURE 17. BER versus phase noise variance at SNR = 10 with channel model B.

significant improvement, as a result of the capability of ISDF to eliminate the residual IMI.

Fig. 17 depicts the BER under different phase noise variance to illustrate the advantages of using PE correction methods. As shown in the figure, without PE compensation, the BER is very bad and the system cannot recover the transmitted data symbols. Applying PE estimation or correction method can significantly improve the BER performance. The ISDF-PNC, ISDF-EKF and ISDF-MBPS methods show significant performance improvement compared with the PNC, EKF and MBPS methods. The MBPS method performs well at low phase noise variance.

IV. CONCLUSION

In this paper, the development and experimental investigation of an FBMC/OQAM physical layer function that is similar to the IEEE 802.11a standard with specially designed pilot locations to suit the FBMC/OQAM waveform are presented. A series of experiments was done to validate the design's capabilities. Measurements of the indoor channel characteristics were conducted and validated using ray tracing method, and then the model was used for simulating the channel. The results show close agreement between the BER of the experimental and simulation results. An investigation was carried out to evaluate the impact of the phase noise. Low complexity methods to compensate for the phase noise have been evaluated experimentally and by numerical simulations. The MBPS method was then optimized to achieve a good trade-off between computational complexity and performance. Moreover, the pilot's power was optimized for efficient phase estimation in the PNC and EKF methods. It is found that the MBPS method performs fairly well at low phase noise and high SNR; however, at high phase noise and low SNR, the PNC and EKF methods can tolerate a much larger phase noise than the MBPS method. In the presence of severe multipath fading, the IMI becomes significant, thus the ISDF technique can be used to eliminate the residual interference and enhance the system performance. It is worth mentioning that the PNC method is a better choice compared to other methods as it has a good trade-off between complexity and performance. An experimental comparison between the WARP and USRP that provides different frequency stability of the oscillator can be done in the future to study the impact of residual CFO on the performance of low-cost SDR-based FBMC/OQAM system.

APPENDIX

The abbreviations used in this paper are listed as:

Acronym	*Definition*
ADC	Analog-to-digital converter.
AFB	Analysis filter banks.
AGC	Automatic gain control.
AWGN	Additive white Gaussian noise.
BB	Baseband.
BPSK	Binary phase-shift-keyed.
BER	Bit error rate.
CFO	Carrier frequency offset.
CIR	Channel impulse response.
CPE	Common phase error.
DAC	Digital-to-analog converter.
EKF	Extended Kalman filter.
FBMC	Filter bank multicarrier.
FEC	Forward error correction.
FFT	Fast Fourier transform.
FSPL	Free-space path loss.
I/Q	In-phase or quadrature component.
IAM	Interference approximation method.
ICI	Inter-carrier interference.
IMI	Intrinsic imaginary interference.
ISDF	Iterative soft decision feedback.
ISI	Inter-symbol interference.
LoS	Line-of-sight.
LS	Least squares.
LTS	Long training sequential.
MBPS	Modified blind phase searching.
MMSE	Minimum mean square error.
MIMO	Multiple-input-multiple-output.
MMSE	Minimum mean square error.
ML	Maximum-likelihood.
NLoS	Non line-of-sight.
OFDM	Orthogonal frequency division multiplexing.
OQAM	Offset quadrature amplitude modulation.
PC	Personal computer.
PDP	Power delay profile.
PSR	Pilot-to-signal-power-ratio.
PN	Phase noise.
PNC	Phase noise compensation.
PPM	Parts per million.
PPN	Polyphase network.
QAM	Quadrature amplitude modulation.
RF	Radio frequency.
RMS	Root-mean-square.
Rx	Receiver.
SDR	Software-defined radio.
SE	Spectral efficiency.

SFB	Synthesis filter banks.
SNR	Signal-to-noise-ratio.
STBC	Space-time block code.
STS	Short training symbols.
Tx	Transmitter.
WARP	Wireless open-access research platform.

REFERENCES

[1] B. Farhang-Boroujeny, "OFDM versus filter bank multicarrier," *IEEE Signal Process. Mag.*, vol. 28, no. 3, pp. 92–112, May 2011.
[2] K. Abdulaziz Alaghbari, H.-S. Lim, and T. Eltaif, "Robust precoder for mitigating inter-symbol and inter-carrier interferences in coherent optical FBMC/OQAM," *IEEE Photon. J.*, vol. 11, no. 4, pp. 1–15, Aug. 2019, doi: 10.1109/JPHOT.2019.2925856.
[3] C. Lele, J.-P. Javaudin, R. Legouable, A. Skrzypczak, and P. Siohan, "Channel estimation methods for preamble-based OFDM/OQAM modulations," *Eur. Wireless*, vol. 9, no. 7, pp. 741–750, 2007.
[4] T. H. Nguyen, F. Rottenberg, S. P. Gorza, J. Louveaux, and F. Horlin, "Efficient chromatic dispersion compensation and carrier phase tracking for optical fiber FBMC/OQAM Systems," *J. Lightw. Technol.*, vol. 35, no. 14, pp. 2909–2916, Jul 23, 2017.
[5] K. A. Alaghbari, H. S. Lim, and T. Eltaif, "An improved least squares channel estimation algorithm for coherent optical FBMC/OQAM system," *Opt. Commun.*, vol. 439, pp. 141–147, 2019.
[6] B. You, L. Yang, F. Luo, S. Fu, S. Yang, B. Li, and D. Liu, "Joint carrier frequency offset and phase noise estimation based on pseudo-pilot in CO-FBMC/OQAM system," *IEEE Photon. J.*, vol. 11, no. 1, pp. 1–11, Feb. 2019.
[7] D. Petrovic, W. Rave, and G. Fettweis, "Common phase error due to phase noise in OFDM-estimation and suppression," in *Proc. IEEE 15th Int. Symp. Pers., Indoor Mobile Radio Commun.*, vol. 3, Barcelona, Spain, Sep. 2004, pp. 1901–1905.
[8] *IEEE Standard for Telecommunications and Information Exchange Between Systems—LAN/MAN Specific Requirements—Part 11: Wireless Medium Access Control (MAC) and Physical Layer (PHY) Specifications: High Speed Physical Layer in the 5 GHz band*, IEEE Standard 802.11a-1999, Dec. 1999, pp. 1–102, doi: 10.1109/IEEESTD.1999.90606.
[9] H. Tang, M. Xiang, S. Fu, M. Tang, P. Shum, and D. Liu, "Feed-forward carrier phase recovery for offset-QAM Nyquist WDM transmission," *Opt. Exp.*, vol. 23, no. 5, pp. 6215–6227, 2015.
[10] T. T. Nguyen, S. T. Le, R. Nissel, M. Wuilpart, L. Van Compernolle, and P. Megret, "Pseudo-pilot coding based phase noise estimation for coherent optical FBMC-OQAM transmissions," *J. Lightw. Technol.*, vol. 36, no. 14, pp. 2859–2867, Jul. 15, 2018.
[11] B. You, L. Yang, F. Luo, S. Yang, D. Chen, Y. Ni, B. Li, and D. Liu, "Pilot-based extended Kalman filter for phase noise estimation in CO-FBMC/OQAM systems," *Opt. Commun.*, vol. 443, pp. 116–122, Jul. 2019.
[12] A. Kakkavas, M. Castañeda, J. Luo, T. Laas, W. Xu, and J. A. Nossek, "FBMC-OQAM with phase noise: Achievable performance and compensation," in *Proc. IEEE 18th Int. Workshop Signal Process. Adv. Wireless Commun. (SPAWC)*, Sapporo, Japan, Jul. 2017, pp. 1–5.
[13] P. Singh and K. Vasudevan, "CFO and channel estimation for SIMO-FBMC/OQAM systems," in *Proc. 23rd Asia–Pacific Conf. Commun. (APCC)*, Perth, WA, Australia, Dec. 2017, pp. 1–6.
[14] P. Singh, E. Sharma, K. Vasudevan, and R. Budhiraja, "CFO and channel estimation for frequency selective MIMO-FBMC/OQAM systems," *IEEE Wireless Commun. Lett.*, vol. 7, no. 5, pp. 844–847, Oct. 2018.
[15] A. Baghaki and B. Champagne, "Joint frequency offset, time offset, and channel estimation for OFDM/OQAM systems," *EURASIP J. Adv. Signal Process.*, vol. 2018, no. 1, p. 4, Jan. 2018.
[16] K. A. Alaghbari, H. Lim, and T. A. Eltaif, "Compensation of chromatic dispersion and nonlinear phase noise using iterative soft decision feedback equalizer for coherent optical FBMC/OQAM systems," *J. Lightw. Technol.*, vol. 38, no. 15, pp. 3839–3849, Mar. 19, 2020, doi: 10.1109/JLT.2020.2981481.
[17] A. Dziri, C. Alexandre, R. Zakaria, and D. Le Ruyet, "SDR based prototype for filter bank based multi-carrier transmission," in *Proc. 11th Int. Symp. Wireless Commun. Syst. (ISWCS)*, Aug. 2014, pp. 878–882, doi: 10.1109/ISWCS.2014.6933477.
[18] J. Baranda, P. Henarejos, Y. Grunenberger, and M. Najar, "Prototyping with SDR: A quick way to play with next-gen communications systems," in *Proc. 8th Int. Symp. Wireless Commun. Syst.*, Nov. 2011, pp. 16–20, doi: 10.1109/ISWCS.2011.6125301.
[19] M. Penner, M. Nabeel, and J. Peissig, "FBMC testbed with frequency domain synchronization and adaptive bandwidth," in *Proc. 17th Int. Conf. Wireless Mobile Comput., Netw. Commun. (WiMob)*, 2021, pp. 423–426, doi: 10.1109/WiMob52687.2021.9606255.
[20] P. Murphy, A. Sabharwal, and B. Aazhang, "Design of WARP: A wireless open-access research platform," in *Proc. 14th Eur. Signal Process. Conf.*, Florence, Italy, Sep. 2006, pp. 1–5.
[21] *WARP V3 Kit*. Accessed: Jul. 17, 2022. [Online]. Available: https://www.mangocomm.com/products/kits/warp-v3-kit/
[22] M. G. Bellanger, "Specification and design of a prototype filter for filter bank based multicarrier transmission," in *Proc. IEEE Int. Conf. Acoust., Speech, Signal Process.*, Salt Lake City, UT, USA, May 2001, pp. 2417–2420, doi: 10.1109/ICASSP.2001.940488.
[23] M. Bellanger, "FBMC physical layer: A primer," Phydyas Project, Europe, Tech. Rep. 06, 2010.
[24] Q. Bai and J. A. Nossek, "On the effects of carrier frequency offset on cyclic prefix based OFDM and filter bank based multicarrier systems," in *Proc. IEEE 11th Int. Workshop Signal Process. Adv. Wireless Commun. (SPAWC)*, Jun. 2010, pp. 1–5, doi: 10.1109/SPAWC.2010.5670999.
[25] M. R. Khanzadi, D. Kuylenstierna, A. Panahi, T. Eriksson, and H. Zirath, "Calculation of the performance of communication systems from measured oscillator phase noise," *IEEE Trans. Circuits Syst. I, Reg. Papers*, vol. 61, no. 5, pp. 1553–1565, May 2014.
[26] A. Mohammadian and C. Tellambura, "RF impairments in wireless transceivers: Phase noise, CFO, and IQ imbalance—A survey," *IEEE Access*, vol. 9, pp. 111718–111791, 2021, doi: 10.1109/ACCESS.2021.3101845.
[27] *Source Code for Implementing FBMC/OQAM on WARP Kit*. Accessed: Sep. 2, 2022. [Online]. Available: https://github.com/khalidxp/Implementing-FBMC-OQAM-on-SDR-WARP-kit
[28] S. T. Le, T. Kanesan, E. Giacoumidis, N. J. Doran, and A. D. Ellis, "Quasi-pilot aided phase noise estimation for coherent optical OFDM systems," *IEEE Photon. Technol. Lett.*, vol. 26, no. 5, pp. 504–507, Mar. 17, 2014.
[29] S. Wu and Y. Bar-Ness, "A phase noise suppression algorithm for OFDM-based WLANs," *IEEE Commun. Lett.*, vol. 6, no. 12, pp. 535–537, Dec. 2002.
[30] M. Speth, S. A. Fechtel, G. Fock, and H. Meyr, "Optimum receiver design for wireless broad-band systems using OFDM. I," *IEEE Trans. Commun.*, vol. 47, no. 11, pp. 1668–1677, Nov. 1999.
[31] T. Nguyen, S. Gorza, J. Louveaux, and F. Horlin, "Low-complexity blind phase search for filter bank multicarrier offset-QAM optical fiber systems," in *Adv. Photon., OSA Tech. Dig.*, Jul. 2016, pp. 1–10, Paper SpW2G.2.
[32] *Channel Measurement Data*. Accessed: Jul. 17, 2022. [Online]. Available: https://github.com/khalidxp/Wireless-channel-measurements-in-FET-MMU-corridor
[33] Z. Ji, B.-H. Li, H.-X. Wang, H.-Y. Chen, and T. K. Sarkar, "Efficient ray-tracing methods for propagation prediction for indoor wireless communications," *IEEE Antennas Propag. Mag.*, vol. 43, no. 2, pp. 41–49, Apr. 2001.
[34] T. K. Sarkar, Z. Ji, K. Kim, A. Medouri, and M. Salazar-Palma, "A survey of various propagation models for mobile communication," *IEEE Antennas Propag. Mag.*, vol. 45, no. 3, pp. 51–82, Jun. 2003.
[35] Z. Yun and M. F. Iskander, "Ray tracing for radio propagation modeling: Principles and applications," *IEEE Access*, vol. 3, pp. 1089–1100, 2015.
[36] *Appendix I.9*, document ITU-T R G.975.1, 2004.
[37] V. Erceg, *IEEE P802.11 Wireless LANs TGn Channel Models*, IEEE Standard 802.11, Zyray Wireless, 11-03/940r4, 2004.

KHALED A. ALAGHBARI received the B.Eng. degree (Hons.) in electronics engineering majoring in telecommunication, and the M.Eng.Sc. and Ph.D. degrees from Multimedia University (MMU), Melaka, Malaysia, in 2011, 2014, and 2020, respectively. His research interests include signal processing for wireless and optical communications and machine learning.

HENG-SIONG LIM (Senior Member, IEEE) received the B.Eng. degree (Hons.) in electrical engineering from Universiti Teknologi Malaysia, in 1999, and the M.Eng.Sc. and Ph.D. degrees in engineering focusing on signal processing for wireless communications from Multimedia University, in 2002 and 2008, respectively. He is currently a Professor with the Faculty of Engineering and Technology, Multimedia University. His current research interests include the areas of signal processing for advanced communication systems, with emphasis on detection, and estimation theory and their applications.

NOR HIDAYATI ABDUL AZIZ received the Graduate degree in electronics engineering majoring in computer from Multimedia University, in 2002, and the master's degree in engineering from Universiti Teknologi Malaysia, in 2005. She is currently pursuing the Ph.D. degree in computational intelligence with Universiti Malaysia Pahang. She has worked at Telekom Malaysia Berhad as a Field Engineer for four years immediately after graduation, and then joined Multimedia University as a Lecturer, after finishing her master's degree. She is also working with the Faculty of Engineering and Technology, Multimedia University, Melaka Campus.

T. BHUVANESWARI (Senior Member, IEEE) received the Ph.D. degree in electronics engineering from Multimedia University, Melaka Campus, in 2013. She is currently working as a Lecturer with Multimedia University. Her research interests include digital system design, VLSI, and solar energy harvesting techniques.

TICK HUI OH (Senior Member, IEEE) received the B.Sc. degree in electrical and electronics engineering and the M.Eng.Sc. degree, in 2001 and 2005, respectively. He is currently a Senior Lecturer with Multimedia University, Melaka, Malaysia. Besides telecommunication, he is also pursuing his interest in renewable and sustainable energy.